

The October 20, 2006 Manyas ($M_L=5.2$) and October 24, 2006 Gemlik ($M_L=5.2$) earthquakes in the Marmara region (NW Turkey): ground motion characteristics

Esref Yalcinkaya,

Istanbul University, Engineering Faculty, Geophysical Engineering, Avcilar, Istanbul, Turkey

Article history

Received March 6, 2014; accepted November 18, 2014.

Subject classification:

Gemlik, Marmara, Site effect, Surface waves within basin, Ground motion.

ABSTRACT

In this study, we analyze the ground motion characteristics of October 20, 2006 Manyas ($M_L=5.2$) and October 24, 2006 Gemlik ($M_L=5.2$) earthquakes. Both earthquakes occurred on the southern branch of the North Anatolian Fault Zone in Marmara region, which has a lower seismic hazard relative to the northern branch. The two events are the largest earthquakes on the southern branch recorded by a modern and vast seismological network; therefore their records are valuable to evaluate seismic risk of the region and the understanding of physics of wave propagation. The analysis show that the attenuation of PGAs is very similar for two earthquakes, but they are not represented by the empirical relation obtained for earthquakes occurred on the northern branch. The waveforms of the Gemlik earthquake recorded by BYTNet array indicate an EW rupture orientation with right-lateral slip which fits to the general character of the southern branch. Ground motions at the stations located within basin are strongly influenced by the presence of locally induced surface waves resulting in lengthening of significant shaking duration with respect to a nearby ridge site. Surface wave characteristics are very similar for the Manyas and Gemlik earthquakes, but variations are observed on components which may be related to 3D basin geometry. Resonance frequencies of the surface waves generated within basin are very close to the 1D site resonances at the stations obtained from H/V ratios of S waves. The resonance frequency is about 0.2 Hz within the large Bursa Plain, whereas it increases to about 0.9 Hz within the smaller Gemlik Plain.

1. Introduction

The North Anatolian Fault Zone (NAFZ) is a dextral strike-slip fault zone extending more than 1600 km-long from Karliova in the east to the Aegean Sea in the west, which forms the northern boundary of the westward moving Anatolian Plate. The Marmara region is located in a transition zone where the right-lateral strike-

slip character of the NAFZ meets with the extensional character of Aegean [Dewey and Sengor 1979, Sengor et al. 1985, Smith et al. 1995]. This transition splits the NAFZ in the Marmara region into two main branches, referred to as northern NAF (NNAF) and southern NAF (SNAF) branches as illustrated in Figure 1. The northern branch starts from south of Akyazi and then passes through the Sapanca Lake, Izmit Gulf, Marmara Sea, Saros Gulf and northern Aegean Sea. On the contrary of its simple structure, the southern branch presents a wider deformation zone including multiple strands [Barka and Kucsu 1996, Kurtulus and Canbay 2007].

The northernmost strand of this deformation zone (hereafter, referred to as southern branch of the NAF) follows the path south of Akyazi, Geyve, Pamukova, south of Iznik Lake, Gemlik, southern coast of Marmara Sea and Kapidag Peninsula, where it makes a left bend and continues southwest in the Biga Peninsula to reach the Aegean Sea (Figure 1). Long-term seismicity, GPS measurements and geological data suggest that the northern branch of the NAFZ is more active than the other two southern branches [Barka 1997]. The GPS studies have indicated that there is an asymmetric slip partitioning between the northern and southern branches of the NAFZ with the northern branch taking much larger motion than the southern branch [Armijo et al. 1999, 2002, McClusky et al. 2000, Meade et al. 2002, Flerit et al. 2003, Nyst and Thatcher 2004]. It has been determined that the NNAF accommodates 20 mm/year of the slip rate caused by the plate kinematics, which is about 24 mm/year, with no strike perpendicular motion, while the rest of the slip rate is accommodated along the southern branch

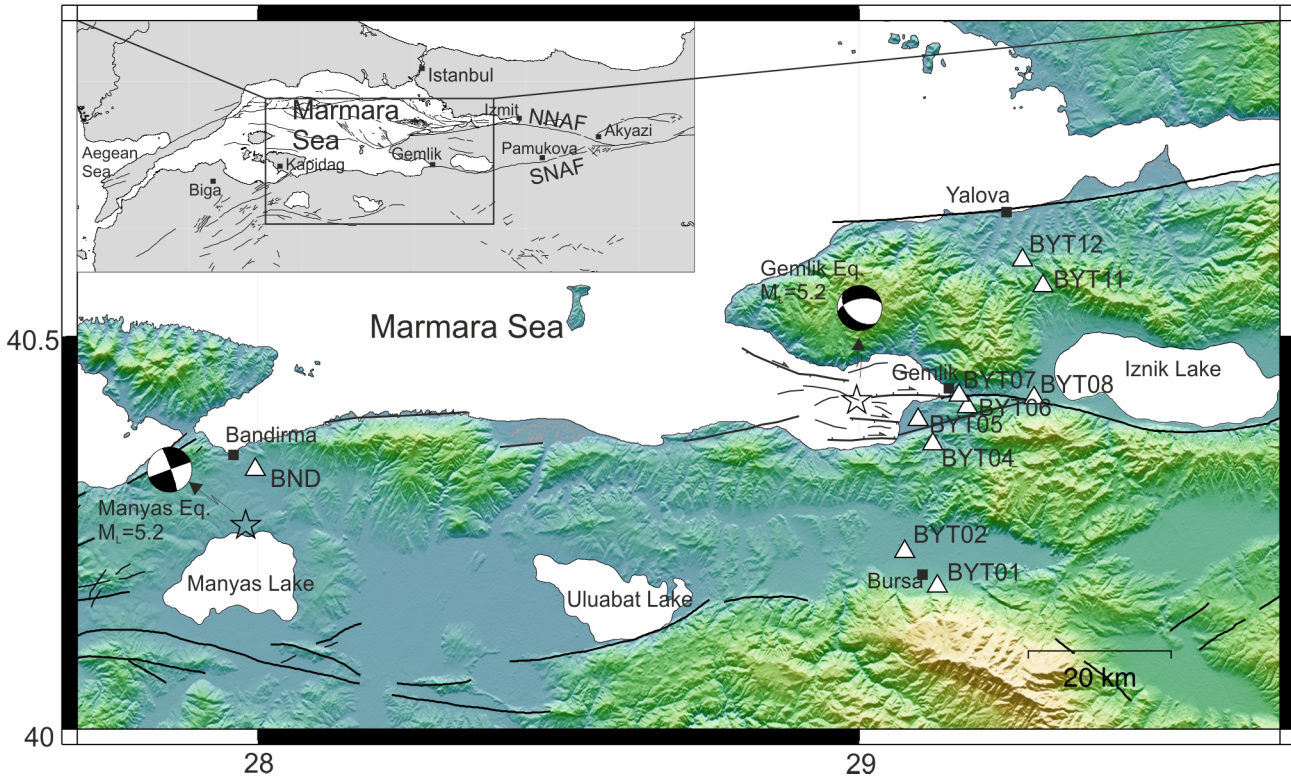


Figure 1. Tectonics of the region (the fault lines are modified from Kuscü et al. [2009], Saroglu et al. [1992] and Le Pichon et al. [2001]) and the locations (stars) of Manyas and Gemlik earthquakes are shown. Source mechanisms of the earthquakes are from Orgulu [2011]. The stations are shown with triangles.

with prominent strike perpendicular motion or extension [Flerit et al. 2003, Nyst and Thatcher 2004]. Strike perpendicular motion is in accordance with the geological observations indicating normal faults along the southern branch [Barka and Kadinsky-Cade 1988, Saroglu et al. 1992].

While all studies have concentrated on the northern branch in the Marmara Sea because of the increasing seismic risk as a result of the 1999 Izmit ($M_w=7.6$) and Duzce ($M_w=7.2$) earthquakes, two moderate earthquakes occurred on the southern branch have also attracted the attention on the southern branch. These are the 20 October 2006 Manyas ($M_L=5.2$) and the 24 October 2006 Gemlik ($M_L=5.2$) earthquakes (Figure 1). The earthquakes caused light damages and significant excitement and panic in the Marmara region. The earthquakes threaten a region with very dense population and high industrial capacity. The distance of the Manyas earthquake to the town of Bandirma is ~ 9 km which has a population of 140,000. The Gemlik earthquake is ~ 15 km away from the town of Gemlik which has a population of 92,000 and ~ 30 km away from the province of Bursa which has a population of 2,700,000 (Figure 1). The Gemlik and Manyas earthquakes are the largest earthquakes recorded on the southern branch with a modern station network. The latest earthquakes larger than M_5 occurred on this branch are the 1983 Biga-Canakkale ($M_s=6.1$), the 1964 Manyas-Balikesir

($M_s=7.0$), the 1953 Yenice-Canakkale ($M_s=7.2$), the 1942 Bigadic-Balikesir ($M_s=6.1$), and the 1935 Erdek-Balikesir ($M_s=6.4$) earthquakes (KOERI catalog, <http://udim.koeri.boun.edu.tr>). We do not have strong motion record for most of these earthquakes, because the first strong motion stations in Turkey were established in the 1970s. Therefore, the records of Manyas and Gemlik earthquakes are extremely valuable in investigating the seismic risk of the southern branch.

The parameters of the Manyas and Gemlik earthquakes are given in Table 1. Focal mechanisms of the earthquakes were published by KOERI shortly after the main shocks, which have dominant strike slip character. The source mechanisms were reevaluated by Karabulut et al. [2011], Orgulu [2011] and Kinscher et al. [2013]. Their results give a dominant normal fault character with strike-slip component, in particular for Gemlik earthquake. In fact, all results reflect the complex tectonic of the region which is an extension together with transform regime [Kuscü et al. 2009]. In addition, it is not easy to decide which one of the nodal planes represents the earthquake rupture. Although the main fault orientations in the region are east-west trending, a lot of small fractures take place in directions with oblique angles to the main trend. Irmak et al. [2007] suggests a rupture plane in N-S direction for Gemlik earthquake depending on aftershock distribution [Tunc et al. 2011]. Kinscher et al. [2013] relates

Date	Time	Epicenter (Lat. / Long.)	Magnitude	Depth (km)	Fault Mech.		
					Strike	Dip	Rake
20.10.2006 Manyas	18:15:24	40.262/27.982	$M_L=5.2$	13.0	158/25	81/79	169/9(KOERI)
		40.245/27.980	$M_w=4.8$	6.0	250/340	90/85	175/0 (O2011)
24.10.2006 Gemlik	14:00:21	40.419/28.996	$M_L=5.2$	14.0	229/137	69/86	-176/-21 (KOERI)
		40.417/28.990	$M_w=4.9$	6.0	260/130	57/45	-123/-50 (O2011)
		40.403/29.001	$M_w=5.2$	8.0	267/153	54/61	-143/-42 (K2011)

Table 1. Parameters of the Manyas and Gemlik earthquakes. KOERI: Kandilli Observatory and Earthquake Research Institute, O2011: Orgulu [2011], K(2011): Karabulut et al. [2011].

Gemlik earthquake with a NE-SW striking fault as a part of pull-apart mechanism which forms the tectonic structure of the region.

Both earthquakes have been recorded by the accelerometers operated by Turkish National Strong Ground Motion Network (Turkish Republic Disaster and Emergency Management Presidency, Earthquake Department) in the region. Aim of this study is to obtain some seismological evidences related with the characteristics of these earthquakes. First we compare the attenuation of the peak ground accelerations (PGA) for the two earthquakes. Then, we evaluate the dependence of waveforms at BYTNet array stations to the site characteristics which may provide significant information about the ground motions around the southern branch of NAFZ.

2. Attenuation of peak ground accelerations

The number of stations operated under the National Strong Motion Network of Turkey increased to 422 in 2013 (<http://kyh.deprem.gov.tr>). Most of the stations are situated on the North Anatolian Fault Zone, the East Anatolian Fault Zone and the graben systems in the Aegean region. The national network is strengthened by small local networks as a result of the different projects in cooperation with universities and municipalities. Some of them are Bursa-Yalova (BYTNet-14 stations), Aydin-Denizli (DATNet-6 stations), Hatay-Kahramanmaras (MATNet-18 station), Eskisehir (ANANet-5 stations) and Izmir (IZNet-16 stations). The most important feature of these local networks is that the distances between the stations are very short and they are able to detect not only the strong earthquakes but also the weaker ones taking place in a targeted region or fault system. In this sense, the ground motion variations can be observed at short distances and their dependence on local geology, fracture mechanism and fracture geometry can be analyzed [Shakal et al. 2006, Wang et al. 2006].

The Manyas and Gemlik earthquakes were recorded by 24 and 30 accelerometric stations, respectively, deployed in the region, including the BYTNet

array stations. Figure 1 shows the locations of strong motion stations closest to the epicenters together with the known faults in the region [Kuscu et al. 2009]. The station parameters and the peak ground accelerations observed at each station are reported in Table 2. The epicentral distances (R_{epi}) range from 9 km to 234 km. BND and BYT05 stations are the closest stations to the epicenters of the Manyas and Gemlik earthquakes, respectively, which both have epicentral distances of 9 km. The largest peak acceleration was 264 cm/s^2 at the BND station during the Manyas earthquake and 206 cm/s^2 at the BYT05 station during the Gemlik earthquake. The Manyas earthquake was recorded only by the EW component sensor at BND station because of failure in the other component sensors. In addition, the EW component record of BND station is suspicious due to a narrow-band amplification in the spectrum around 12 Hz, which was pointed in Figure 2. We think that this amplification is related with the response of the concrete pedestal on which the sensor was mounted. Similar effects caused by instrument pile were observed on the records of some other earthquakes, e.g. Chi-Chi, Taiwan earthquake [Wen et al. 2001], Bingol, Turkey earthquake [Akkar et al. 2005]. Figure 2 compares the EW component records of the two earthquakes at BND and BYT05 stations in time and frequency domains. The two earthquakes present very similar waveforms and spectral shapes on the near-source recordings with small amplitude differences.

In Figure 3, the PGA values representing the geometrical mean of the horizontal components recorded after the Manyas and Gemlik earthquakes are compared with two ground motion prediction equations (GMPE); one of them is obtained from the local recordings [OZ2004: Ozbey et al. 2004], while the other one was derived from the regional recordings [AB2010: Akkar and Bommer 2010]. The GMPE of Ozbey et al. [2004] was established using 195 recordings at distances up to 200 km using earthquakes with $MW \geq 5$, occurred on the northern branch of NAFZ; mostly aftershocks of the 1999 Izmit and Duzce earthquakes including the

Station Code	Lat./Long.	R_{epi} (km) Manyas/Gemlik	PGA(cm/s ²) Manyas/Gemlik	V_{S30} (m/s) (EC8)
ANA01	39.814 / 30.529	223 / 147	1.6 / 4.1	237(C)
ANA02	39.791 / 30.498	221 / 146	0.8 / 1.8	328(C)
ANA04	39.773 / 30.514	223 / 148	1.9 / 3.1	248(C)
ANA05	39.723 / 30.533	- / 152	- / 1.5	?
AYV	39.311 / 26.686	152 / 233	1.4 / 0.9	387(B)
BLC	40.149 / 29.961	169 / 87	1.5 / 2.2	902(A)
BLK	39.650 / 27.856	68 / 130	2.0 / 2.2	662(B)
BLKS	39.642 / 27.875	68 / 129	1.7 / 2.4	460(B)
BND	40.331 / 27.996	9 / 86	263.9 / 5.7	321(C)
BOZ	39.907 / 30.031	179 / 105	2.3 / 3.2	402(B)
BYT01	40.182 / 29.130	98 / 29	3.9 / 36.6	457(B)
BYT02	40.226 / 29.075	93 / 23	10.5 / 77.4	249(C)
BYT04	40.363 / 29.122	98 / 12	12.0 / 179.8	301(C)
BYT05	40.394 / 29.098	96 / 9	11.7 / 206.2	176(D)
BYT06	40.410 / 29.180	104 / 16	9.2 / 100.4	366(B)
BYT07	40.425 / 29.167	103 / 15	11.9 / 95.3	229(C)
BYT08	40.422 / 29.291	113 / 25	16.6 / 45.2	349(C)
BYT11	40.564 / 29.306	118 / 31	10.3 / 29.3	388(B)
BYT12	40.596 / 29.271	- / 31	- / 37.8	358(C)
CNK	40.141 / 26.399	135 / 223	2.4 / 1.7	192(C)
DKL	39.074 / 26.888	- / 234	- / 1.9	193(C)
DMR	39.035 / 28.648	148 / 157	4.4 / 8.8	336(C)
DRSB	39.577 / 28.632	94 / 99	2.8 / 3.3	561(B)
GDZ	38.994 / 29.400	185 / 162	2.1 / 3.0	343(C)
GNN	40.113 / 27.642	33 / 120	4.0 / 1.7	397(B)
INO	39.907 / 30.145	189 / 113	0.7 / 2.5	280(C)
KLS	39.911 / 29.238	114 / 60	6.0 / 10.2	412(B)
KUT	39.428 / 29.992	- / 139	- / 6.3	267(C)
MKP	40.037 / 28.393	- / 67	- / 4.8	265(C)
SMV	39.092 / 28.978	- / 147	- / 3.9	259(C)

Table 2. Station parameters and peak ground accelerations (PGA) for the Manyas and Gemlik earthquakes.

mainshock records as well. The GMPE of Akkar and Bommer [2010] was derived using 532 strong motion accelerograms from Europe and the Middle East, recorded at distances up to 100 km from 131 earthquakes with moment magnitudes ranging from M_5 to 7.6. The GMPEs and their confidence limits are plotted for a strike-slip event with $M_W = 5.0$ earthquake and for stiff soil conditions, because the stations we used are mostly located on the site classes of B or C accord-

ing to the Eurocode EC8 site classification (Table 2). As shown in Figure 3, the attenuation of PGAs for both earthquakes is very similar. The AB2010 predictions of the peak accelerations observed during the Manyas and Gemlik earthquakes are better than the OZ2004 predictions. This may imply that the attenuation of the PGAs on the southern branch may not be similar to the northern branch. The change in the tectonic regime from strike-slip to trans-tension from north toward the

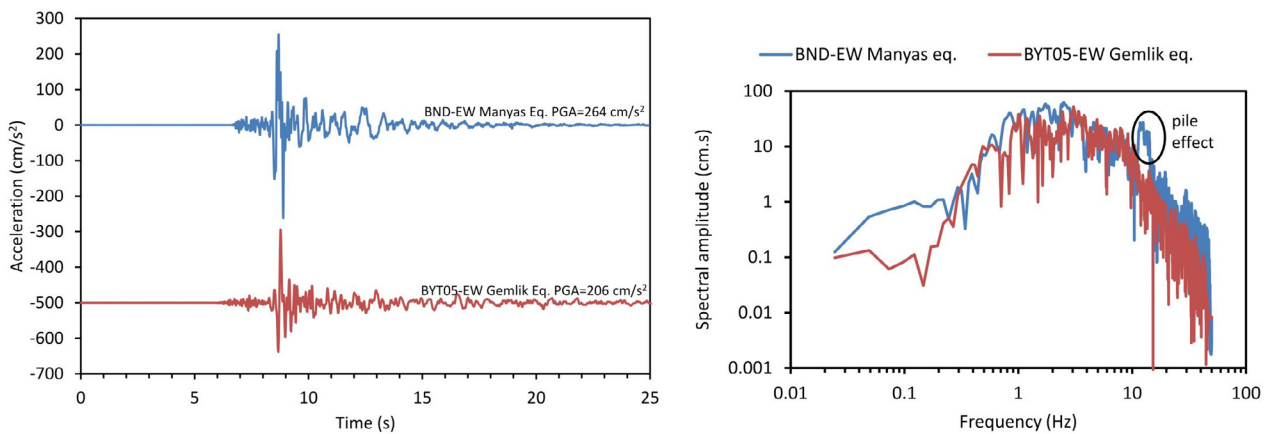


Figure 2. EW component waveforms (left) and spectra (right) of the Manyas (blue line) and Gemlik (red line) earthquakes recorded at BND and BYT05 stations, respectively, are compared. The amplification around 12 Hz caused by instrument pile effect was pointed on the spectrum of BND station.

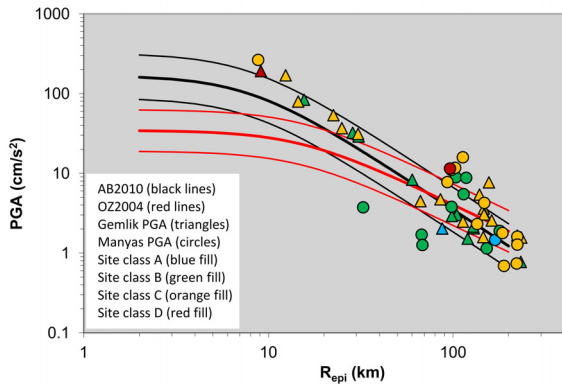


Figure 3. Attenuation of PGAs of Manyas and Gemlik earthquakes are compared with the empirical relations given by Akkar and Bommer [2010] (AB2010), and Ozbey et al. [2004] (OZ2004). The GMPEs (thick lines) and ± 1 standard deviations (thin lines) are plotted for a strike-slip $M_W=5.0$ earthquake and stiff soil conditions. Color codes are given in the graph legend.

south may have created tectonic deformation patterns resulting in such differentiation in the attenuation curves. However, we should keep in mind the points that OZ2004 was derived from a smaller data set than that of AB2010 curve, and the 1999 Izmit earthquake records dominating the OZ2004's data are characterized with low-PGA values; the fact which is still under debate [Ozbey et al. 2004, Miksat et al. 2005, Yalcinkaya et al. 2012]. On the other hand, the observed PGAs during the Gemlik and Manyas events are slightly underestimated by AB2010 at closer distances.

3. The characteristics of waveforms along the BYT-Net array stations

3.1 Near-surface geological and geophysical features beneath the stations

In strong ground motion analysis we generally focus on analyses of peak values. However, dense instrument arrays allow investigating the spatial changing of waveforms and frequency contents. The Manyas and Gemlik earthquakes were recorded at 8 and 9 BYTNet stations, respectively. The BYTNet array totally consists of 14 accelerometric stations which are equipped with digital instruments (Kinometrics Episensor with Etna 24 bits digitizers). The array crosses the SNAF in N-S direction between Yalova and Bursa cities (Figure 4). Two of the stations (BYT11 and BYT12) are located on the northern side of the SNAF, while three of the stations (BYT01, BYT02 and BYT04) are located on the southern side of the SNAF. BYT05, BYT06, BYT07 and BYT08 stations are nearly on the fault zone. The station locations can be characterized according to geo-morphological and geophysical characteristics obtained from a limited number of studies [Sandikkaya et al. 2010]. A part of this information comes from a study of site investigation made

after the installation of the stations and released in the web page of the network (<http://kyh.deprem.gov.tr/bytnet/bytmetr.htm>). The BYT01 station situates on the slope of the Uludag Mountain in southern side of Bursa Plain. The results from a shallow exploration study carried out on the station location point out to a transition zone including a complex unit with gravelly, sandy, and clayey. S wave velocities increase from 260 m/s at surface to 588 m/s at 19 m depth. The BYT02 station takes place in the mid of the Bursa Plain which consists of thick sediments with Quaternary age and S wave velocity in the top 30 m is 249 m/s. The BYT04 station is deployed in a narrow valley among mountains composed of rock units with Tertiary age. The young sediments underlying the station are about 15 m of thickness, and their S wave velocity is 301 m/s. The BYT05 is located on alluvium with Quaternary age. S wave velocities in surface layers are about 176 m/s. The BYT06 station is operated on a ridge where the units from surface to depth consist of young sediments, Eocene flysh and Paleozoic basement. The S wave velocity in the top 30 m is 366 m/s. The BYT07 station is installed within the Gemlik Plain on alluvium units. The S wave velocity in the plain are very low (~ 229 m/s), and the sediment layer is very thick. The BYT08 station is operated within the Iznik basin. The station locates on continental sediments with Pliocene age. The S wave velocity at this site is about 349 m/s. The BYT11 and BYT12 stations are located on slopes of the Samandag Mountain. The geological units underlying the BYT11 station are clay, claystone, sandstone. BYT12 station overlain travertine rocks and S wave velocity in the top 30 m is 358 m/s.

3.2. BYTNet array waveforms

Acceleration, velocity and displacement time histories of the Gemlik earthquake recorded by BYTNet array stations are shown in Figure 5. All records start 2 seconds before the P wave arrivals due to unreliable onset time of the records, and continue 20 seconds where the seismic wave energy nearly reduces to the noise level, in particular on the acceleration recordings. The records were filtered by Butterworth band pass filter between 0.1-25 Hz before deriving the velocity and displacement records from the acceleration records to avoid baseline offset. The largest amplitudes are observed at BYT04 and BYT05 stations which are the closest stations to the epicenter. Strong S wave pulses, possibly related with source effect are present at the beginning of strong shaking, which are typical of near-fault motions and import significant input energy to structural systems. The PGAs of EW components are slightly higher than those of NS components, in particular at the stations close to the epicenter.

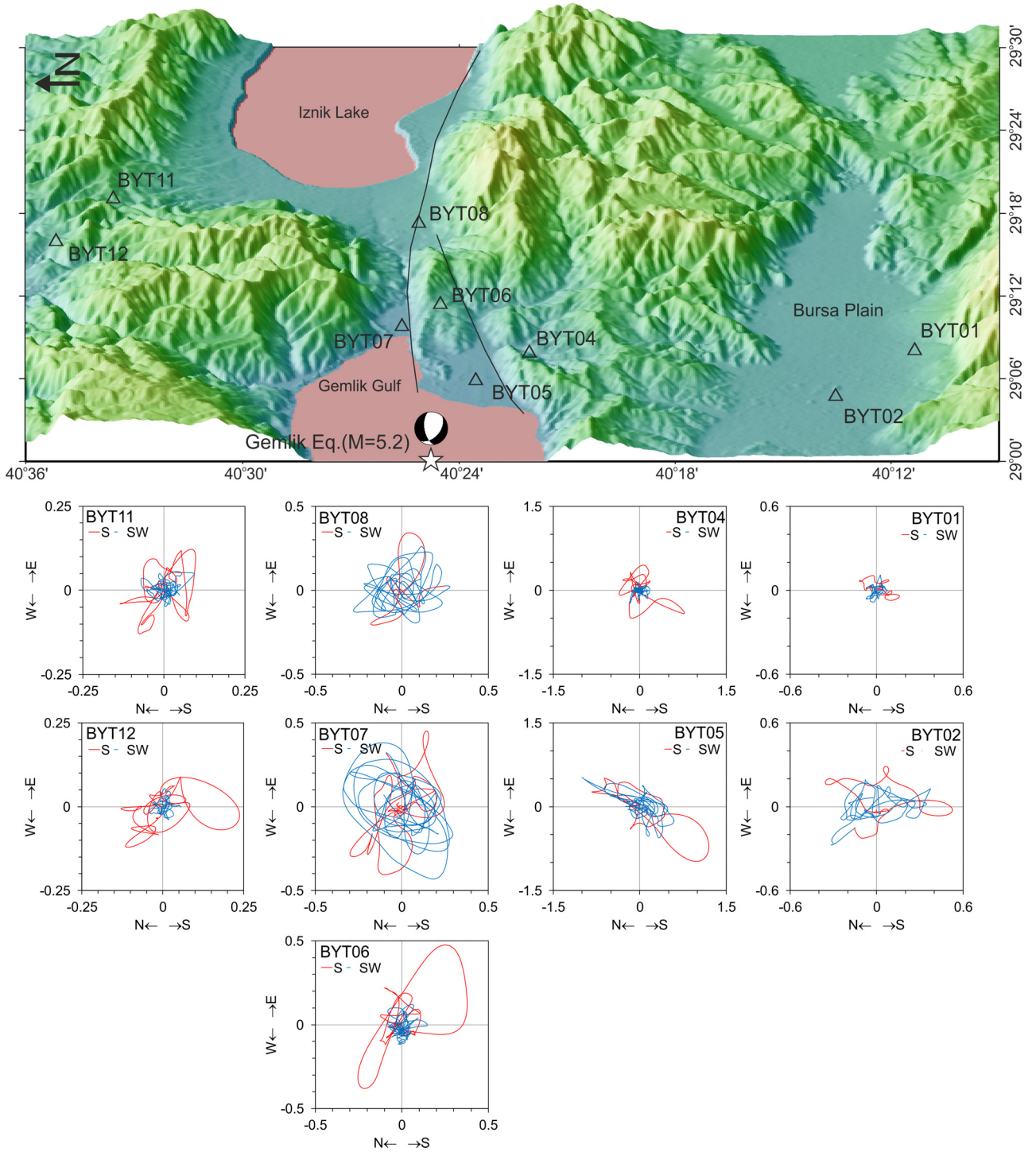


Figure 4. 3D projection map of the study area (view from west). The locations of BYTNet array stations (triangles), the epicenter (star) and the source mechanism of Gemlik earthquake given by Orgulu [2011] are shown on the map. The horizontal plane particle motions (red line for S wave and blue line for surface wave) at each station are shown below the map. The particle motion graphs are arranged according to the map view and the amplitude scales are adjusted within the station groups to view easily the wave orientations.

The acceleration waveforms do not show so much variation among the stations except for the amplitudes, whereas the velocity and displacement waveforms present some important characteristics. S wave polarities can be easily followed on the displacement traces. The initial S wave polarities (filled with grey color in Figure 5) are southward (negative) on the NS components of all stations. On the EW components, S wave polarities reverse

between BYT05 and BYT06 stations. S wave polarities for sites south of BYT05 station are westward (negative), whereas they are eastward (positive) for sites north of BYT06 station. It is difficult to interpret rupturing characteristics from S wave polarities because S wave motion converges toward the T axis and diverges from the P axis, does not have nodal planes. However, reversal of S wave polarities on EW components may be an in-

MANYAS AND GEMLIK EARTHQUAKES IN MARMARA

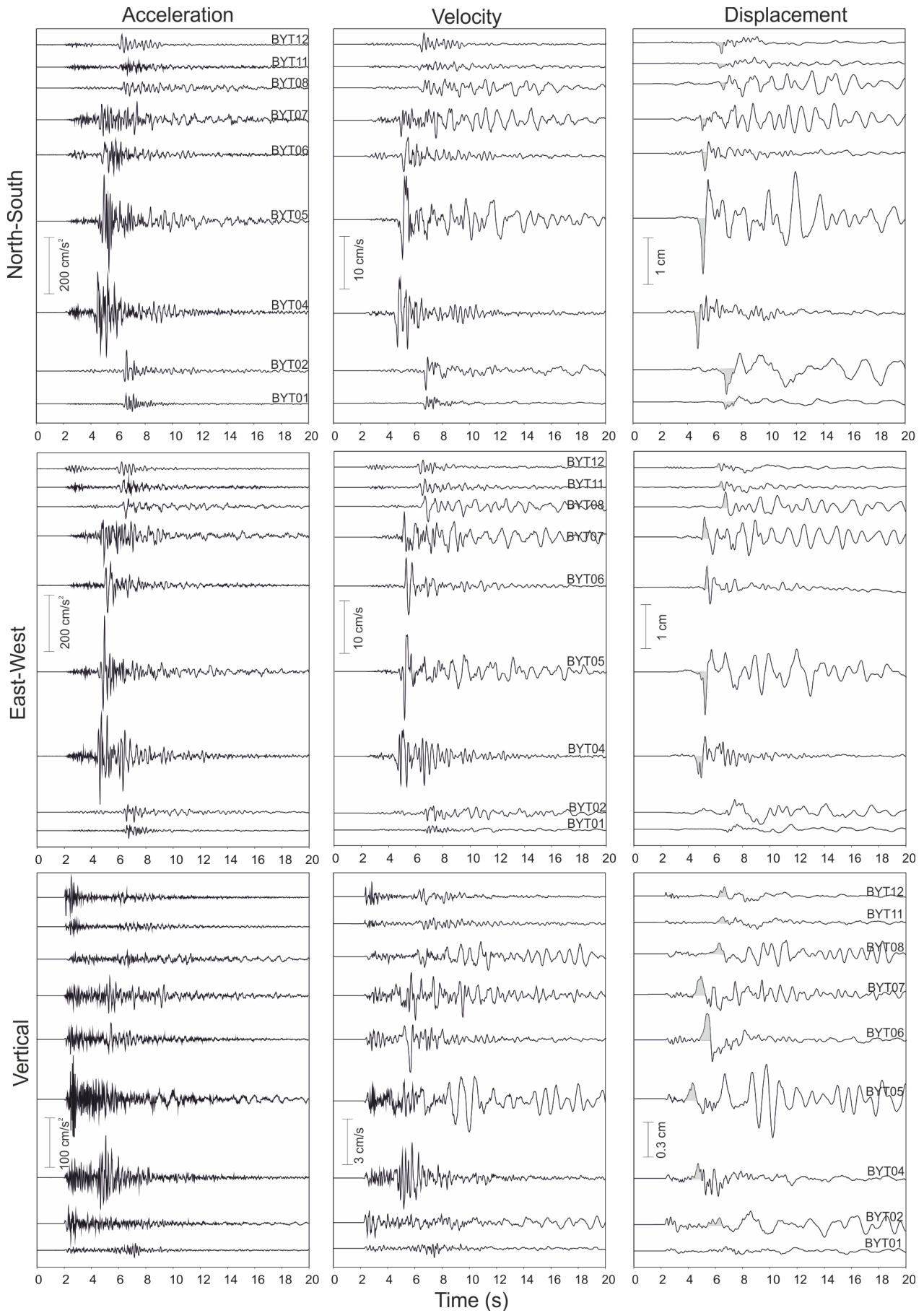


Figure 5. Acceleration (left), velocity (center) and displacement (right) time histories of the Gemlik earthquake recorded at the BYTNet stations. All records start 2 sec before the P arrivals. Different amplitude scale is used for the vertical components and the horizontal components to easily notice the S wave polarizations and the surface wave phases.

dicative of a rupturing orientation falling between the BYT05 and BYT06 stations, nearly east-west direction and right-lateral fault slip. In that case, the ground motions become eastward and westward at the stations staying in the north and south of the fracturing, respectively. This rupture orientation is in accordance with the general character of SNAF and it is about 10 degrees from the fault strike given by Orgulu [2011]. The vertical component records show a coherent upward pulse at all stations. The displacement amplitudes of the vertical components are less than the horizontal component motions, which indicate that the vertical slip of the fault is not as large as expected from the source mechanism solution.

In Figure 4, the particle motions on the horizontal plane at each station are shown below the map. We used two time windows for the particle motions with different line colors which represent S (red line) and surface wave (blue line) phases individually. They were windowed manually from the displacement traces. The width of S wave window was chosen about 3-4 s and the rest of the record was used for the SW window. The particle motions were plotted with different amplitude scales to see the motion orientation at each station clearly. As can be seen in the Figure 4, S wave motions are nearly in E-W direction at the BYT06, BYT07 and BYT08 stations located just to the east of the epicenter. This observation confirms a fault motion with E-W direction indicated earlier from the polarization of S waves. S wave orientations are in NW-SE direction at the northernmost stations, whereas they are in NE-SW direction at the southernmost stations. As the distance to the fault increases, the S wave motions become perpendicular to the wave propagation path as expected.

3.3 Surface waves in BYTNet array

In Figure 5, the presence of low frequency arrivals after S wave is easily distinguished on the velocity and displacement records. These secondary phases at BYT02, BYT05, BYT07 and BYT08 stations have large amplitudes, comparable to those of the S waves. On the other hand, at BYT01, BYT04, BYT06, BYT11 and BYT12 stations the secondary arrivals are not observed at all. This comparison provides evidence for the presence of locally induced low frequency surface waves. To characterize surface waves more clearly the displacement records of two close stations are combined in Figure 6. In the couples of BYT01-BYT02, BYT04-BYT05, BYT06-BYT07 and BYT06-BYT08, the stations are close to each other and one of them is located within the basin (i.e. BYT02, BYT05, BYT07 and BYT08), while the other is located on the ridge (i.e. BYT01, BYT04, and BYT06). In addition, in the couple of BYT11-BYT12, both the stations situate on the

slope of the ridge. The topographic characteristics of the station locations are portrayed in Figure 4. It is obvious that the source and the path effects are not so different for all the station pairs except for the couple of BYT06-BYT08, because these stations are 9 km apart, so the effect of geometric spreading may have caused to amplitude differences at these stations, but still we observe the surface wave effects. In result, one of the stations in the pairs is located on ridge and can be used as a reference for the one located within the basin, in order to assess relative amplifications and surface waves caused by basin edges. We should accept the fact that these reference sites may not meet the ideal reference site conditions to determine real site effects, such that it should be located on rock with no topographic effect. In addition, Table 2 shows that they do not have very different VS30 values. At these stations, site effects will be determined in the following sections by using H/V analysis [Nakamura, 1989]. In conclusion, our first goal is to distinguish the effects of surface waves on the records by comparing the stations.

Several studies [e.g. Graves et al. 1998, Chavez-Garcia and Faccioli 2000, Olsen 2000, Makra et al. 2001, Hruby and Beresnev 2003, Choi et al. 2005] have shown that ground motion within sedimentary basins is strongly influenced by the interaction between the incoming body waves and the 2D/3D structure of a basin's edge. It is known from numerical [e.g. Bard and Bouchon 1980a, b, Reipl et al. 2000, Yalcinkaya and Alptekin 2005a] and experimental [e.g. Kawase 1996, Field 1996, Yalcinkaya and Alptekin 2005b] studies that finite lateral extent of soil surface layers may generate surface waves travelling within basin. The basin edge induced surface waves cause both a lengthening of the significant shaking duration and an increase in the peak values with respect to a nearby ridge site.

In this study, the presence of surface waves at the stations located within basin (red lines in Figure 6) is clearly observed in the form of wave trains with large amplitude following S waves. The displacement records obtained on the ridge sites (black lines in Figure 6) show that the major S wave energy lasts about 3-4 sec, followed by the later displacements reduced to the noise level. In contrast, the later displacement amplitudes at the stations installed within the basin continue until the end of the record with small reduction in amplitudes, due to the contribution of the surface waves. Surface waves are observed on the three components of motion, but their amplitudes are generally weaker on the vertical component. Modeling studies [e.g. Narayan 2005] show that incident SH waves generate Love waves propagating from basin edge and they are recorded on the transverse component, while P and SV waves generate Rayleigh waves which are

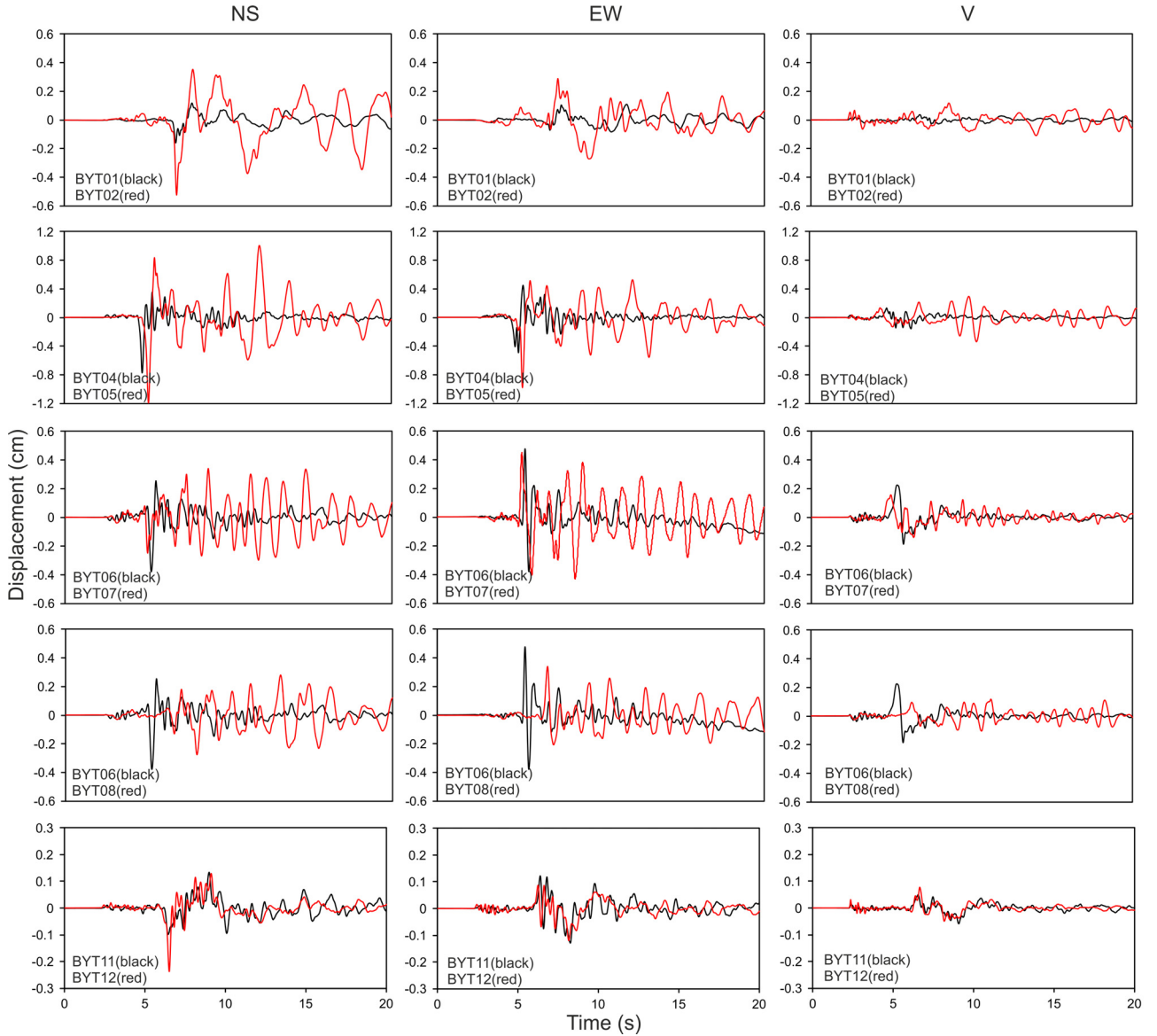


Figure 6. Displacement records of Gemlik earthquake are compared between the station couples. All records start 2 sec before the P arrivals. The red line records represent the stations located within basin, while the black line records represent the stations located on ridge, except for the couple of BYT11-BYT12 which both is located on ridge.

recorded on the radial and vertical components. Therefore, we suggest that the surface waves in Figure 6 consist of mainly Love waves. The particle motions of surface waves on the horizontal plane (blue lines in Figure 4) present a nearly circular motion, in particular at BYT07 and BYT08 stations, which caused by 90 degrees phase difference between the horizontal components. In fact, each station presents a peculiar amplification and surface wave character reflecting soil characteristics depending on the location where it is. At BYT02 station, the amplitudes are greater than those of BYT01 along whole record at the three components. Basin edge induced surface waves at BYT02 station, as it can be monitored on the waveforms, have longer periods relative to those of other stations. In the next section we deal with this long period character emerged on the spectral ratios of BYT02. A plausible reason could be the fact that BYT02 station locates in the

middle of Bursa plain which has larger dimensions relative to the other basins founding in the region (Figure 4). At BYT05 station, the surface waves are observed in the form of packets. S waves amplitudes on the vertical component of BYT05 are not amplified by basin layers relative to those of BYT04, contrary to the amplifications observed on the horizontal components. Similarly, S wave amplitudes at the stations of BYT06 and BYT07 are not so different at all components, but surface wave trains is very clear on the recordings of BYT07 station. Clear surface wave trains are observed on the recordings of BYT08 as well. The displacement records of the BYT11-BYT12 stations located on the ridge match very well and as expected they do not include surface waves.

Similar surface wave characteristics are also observed on the recordings of BYTNet stations during the Manyas earthquake which are not shown here due to

limited space. However, the two earthquakes were compared by computing spectral ratios for the station pairs (Figure 7). The spectral ratios were computed by using the last part of the records with a window length of about 10 s chosen after the main S wave energy from the displacement traces. Therefore, the ratios show es-

pecially the characteristics of surface waves generated within basin. The Fourier spectra of the records were smoothed before spectral ratio estimations using Konno and Ohmachi [1998] algorithm, fixing the relevant parameter b to 20. The spectral ratios for the two earthquakes are given in Figure 7 except for BYT12 be-

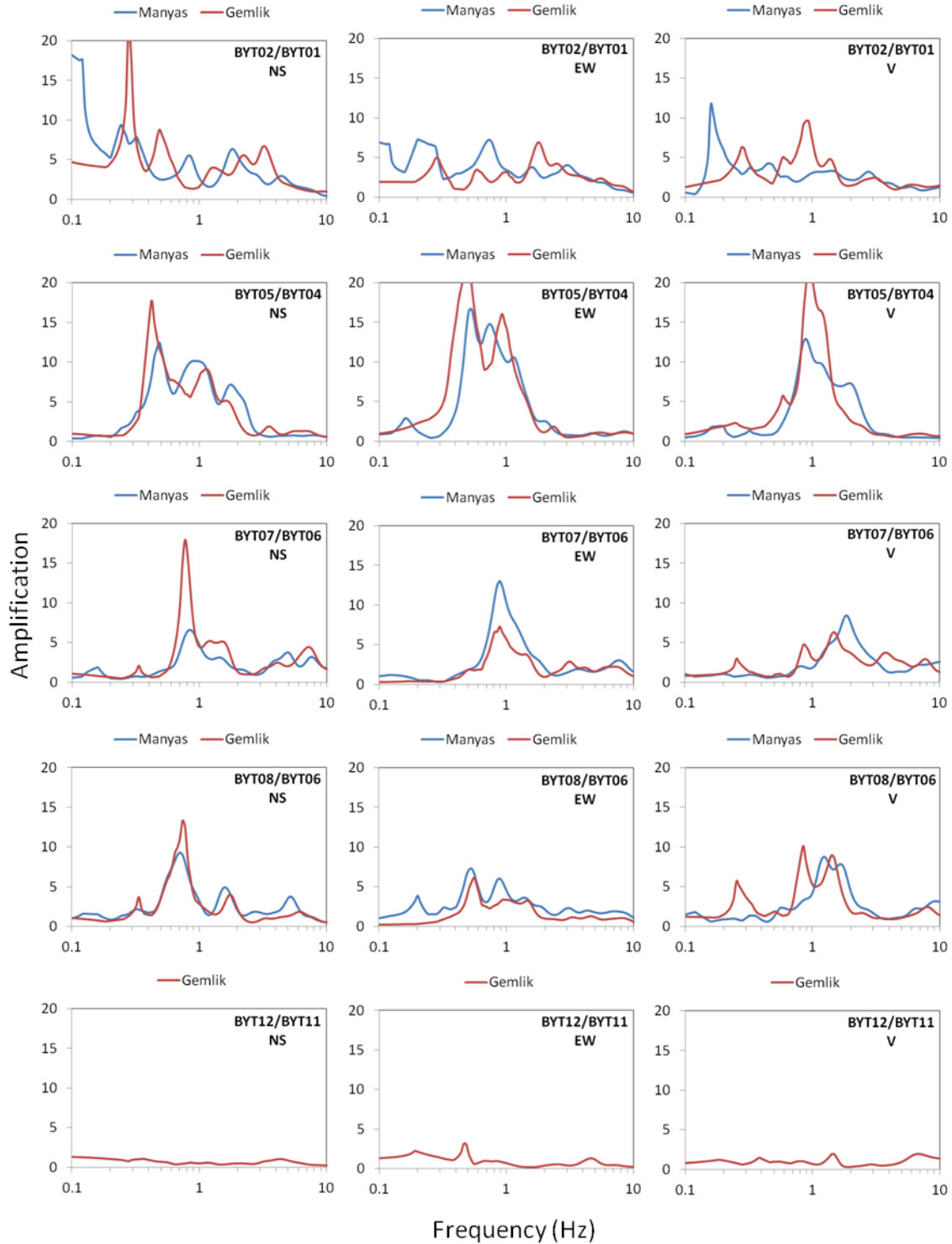


Figure 7. Three component spectral ratios computed for the station couples (BYT01, BYT04, BYT06, BYT11 and BYT12) used as reference for the ones located within basin (BYT02, BYT05, BYT07 and BYT08). Only the surface wave part of the displacement records is used in the ratios. The spectral ratios of Manyas and Gemlik earthquakes are represented by blue and red lines, respectively.

cause it recorded only the Gemlik earthquake. In general, it should be first noted that the spectral ratios are very close for each earthquake. That is, the basin structure underlying the stations generates surface waves in a similar character for the two earthquakes, but the components may reveal different responses. The basin geometry and the angles of incoming waves may cause this variation on the components. The distinguishable peaks showing the frequency and amplitude characteristics of surface waves can be found, in particular on the horizontal components, at about 0.3 Hz, 0.5 Hz, 0.9 Hz, and 0.6 at BYT02, BYT05, BYT07 and BYT08 stations, respectively. The lowest peak frequency is observed at BYT02 station located in the Bursa Plain which has the largest dimensions within the study area, while the highest peak frequency is observed at BYT07 station located in the Gemlik Plain which has the smallest dimensions. Therefore, it can be concluded that the peak frequency of surface waves caused by basin edges depends on the geometrical characteristics of basin besides mechanical properties [Bard and Bouchon 1980a,b]. That is, the basins which have a greater dimensions

cause the surface waves at lower frequencies. The vertical components also show significant peaks at higher frequencies, about 1-2 Hz, relative to the horizontal components although they have smaller amplifications. The surface waves observed on the vertical components are Rayleigh waves simply because they have elliptical particle motion in a vertical plane.

Finally, in order to see site resonance frequencies at these stations, we computed H/V ratios [Nakamura 1989] by using all the available earthquake data recorded at the stations we deal with. The data mainly consist of weak motions obtained from near-small or moderate-distant earthquakes. BYT11 station has the minimum number of earthquake data which is 5, while the BYT05 has the maximum number of earthquake record which is in total 15. H/V ratios have been computed for S waves chosen from acceleration records with different window lengths. As can be seen in Figure 8, all stations except for BYT01 present important resonance peaks. Some of them are the ridge stations which have own site responses as we mentioned earlier. H/V curves of the stations located within the basins, which are

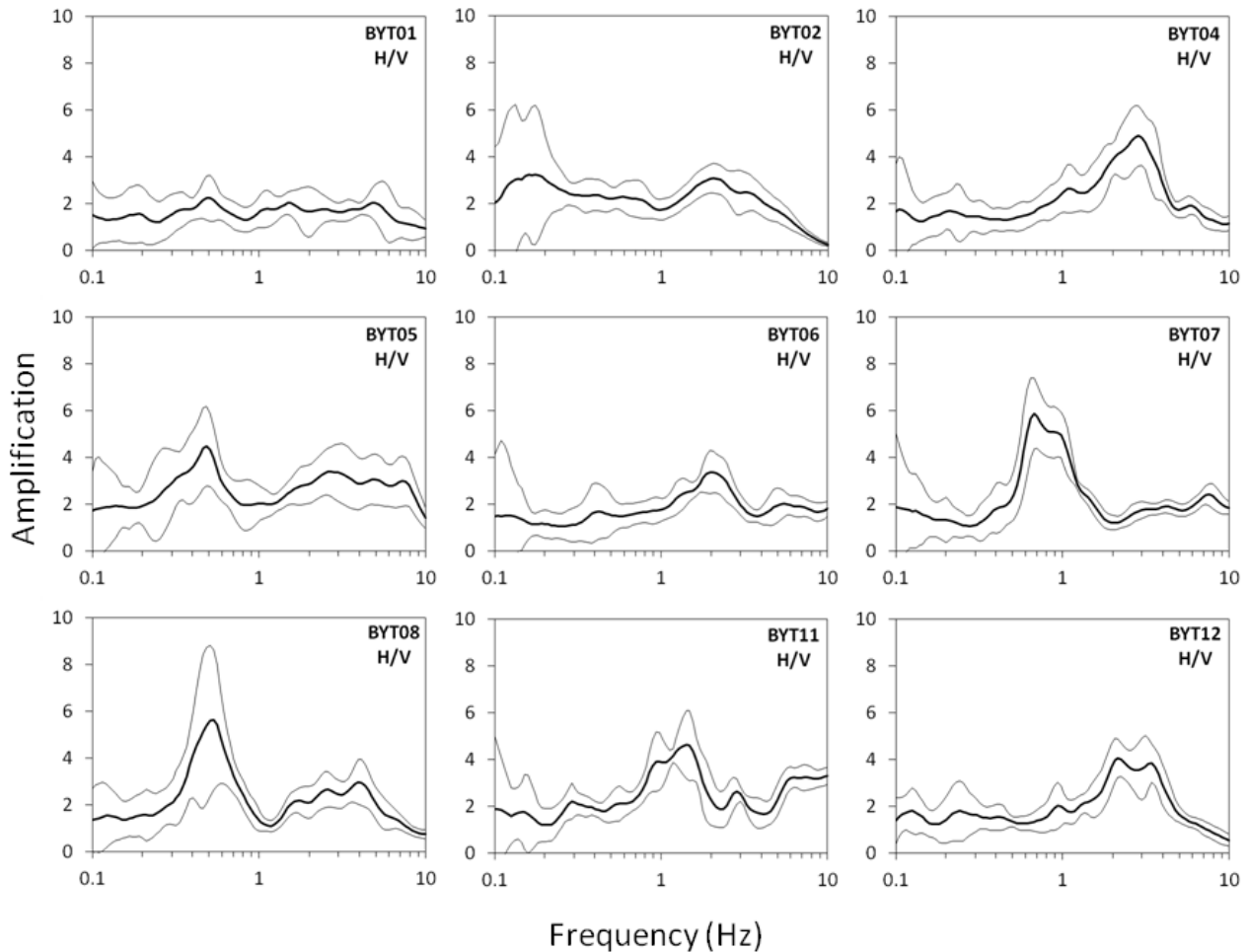


Figure 8. Horizontal-to-vertical spectral ratios (H/V) are computed using S waves of the earthquakes recorded at each station. Thick and thin lines represent the average and ± 1 standard deviation curves, respectively.

BYT02, BYT05, BYT07 and BYT08, present clear site resonance peaks at about 0.2 Hz, 0.5 Hz, 0.7 Hz and 0.5 Hz, respectively. Actually, these resonance frequencies are not so different from that of surface waves. Makra et al. [2005] showed that the frequency of locally generated surface waves coincides with that of 1D resonance. As for the resonance peaks appearing at the stations located on the ridge (BYT04, BYT06, BYT11, BYT12), we claim that since these stations are not located directly on rock the resonance peaks reflect the weathered surface layers.

4. Conclusions

The southern branch of NAFZ in Marmara region undertakes a smaller fraction of the total slip of the main fault compared to the northern branch. In addition, the motion on the southern branch is mainly strike perpendicular or oblique to the strike due to the effect of extensional character of the Aegean region caused by the subduction of the African plate beneath the Aegean. To sum up, the strain accumulation and seismic activity on the southern branch is lower than the northern branch. However, large earthquakes (e.g. 1953 Yenice-Canakkale earthquake $M=7.2$) which may rarely occur on the southern branch constitute a significant risk for the region accommodating high population and industry. Manyas and Gemlik earthquakes which are two significant earthquakes occurred on the southern branch provide a valuable opportunity to examine the source-related effects and site response of strong motion stations.

The two earthquakes produce similar time histories and frequency contents at near-source stations. The observed PGA values are outside one standard deviation of the Akkar and Bommer [2010] relation, at distances lower than 15 km, although it generally represents the PGA values very well at longer distances. Therefore, high accelerations especially in short distances should be taken into account in earthquake resistant design of structures. The attenuation of the PGAs for the two earthquakes are very similar, but they do not fit the empirical relation obtained from the earthquakes occurred on the northern branch [Ozbey et al. 2004]. The reason of attenuation variation may be due to the different tectonic structures between the two strands which in turn may result in different level of deformation of the crust around the northern and the southern branches of the North Anatolian Fault Zone. On the other hand, it should be taken into account that the relation of Ozbey et al. [2004] is based on a smaller dataset mainly from the 1999 Izmit earthquake which is characterized with the low-PGA values.

The recordings of Gemlik earthquake obtained on

the near-field network, BYTNet, provide an opportunity to see the source-related effects. Large S wave pulses observed in the beginning of strong shaking are very important in terms of seismic energy affecting the structures. The polarity change of S waves on EW components between BYT05 and BYT06 stations reveals a rupture orientation in nearly E-W direction which is in accordance with the general trend of SNAF zone. BYTNet stations present significant site effects reflecting the local geology and the site geometry where the stations are located on. Surface waves following S waves with large amplitudes are observed at the stations located within the basin. Their waveforms show variations at the stations in the form of wave trains or wave groups. This may reflect the locations where they occurred and/or wave interference within basin structure. Surface wave amplitudes are larger on horizontal components pointing out that they mainly consist of Love waves. In the frequency domain, the energy of surface waves is observed at low frequencies, about 0.3 Hz, in the Bursa Plain which has larger dimensions. On the other hand, in a small basin, the Gemlik Plain, the peak frequency of the surface waves raises to about 0.9 Hz. The characteristics of basin edge induced surface waves do not present any significant variation for Manyas and Gemlik earthquakes. However, the peak frequencies and amplifications show variations on components. The peak frequencies are observed at higher frequencies on vertical components in general. 3D geometry of the basins and the type of surface waves may be causing these variations. The H/V ratios at the stations located within basin give the site resonance frequencies similar with the peak frequencies of surface waves as it is expected from theoretical studies [Makra et al. 2005]. The sediment thickness in the Bursa Plain is about 300 m [Imbach 1997]. In such case, it yields site resonance frequency of 0.25 Hz assuming average sediment S wave velocity of 300 m/s. It is very close to that obtained from H/V ratios.

As a result, the seismological observations of Manyas and Gemlik earthquakes provide some significant clues about both the character of the southern branch earthquakes and the ground motions that could affect the region. We need more observations to strengthen these clues and new studies to reveal basin structures. A large earthquake on the southern branch may cause high damage in the cities settled within basins.

Acknowledgements. I thank two anonymous reviewers for helpful comments. I also acknowledge Ali Pinar who kindly improved the English of the paper. A special thank to Earthquake Department of Turkish Republic Disaster and Emergency Management Presidency for providing earthquake data.

References

- Akkar, S., D. Boore and P. Gulkan (2005). An evaluation of the strong ground motion recorded during the May 1, 2003 Bingol Turkey, Earthquake, *Journal of Earth Engineering*, 9(2), 173-197.
- Akkar, S. and J.J. Bommer (2010). Empirical equations for the prediction of PGA, PGV and spectral accelerations in Europe, the Mediterranean region and the Middle East, *Seismological Research Letters*, 81, 195-206.
- Armijo, R., B. Meyer, A. Hubert and A. Barka (1999). Propagations of the North Anatolian Fault into the Northern Aegean: timing and kinematics, *Geology*, 27(3), 267-270.
- Armijo, R., B. Meyer, S. Navarro, G. King and A. Barka (2002). Asymmetric slip partitioning in the Sea of Marmara pull-apart: a clue to propagation processes of the North Anatolian Fault?, *Terra Nova*, 14(2), 80-86.
- Bard, P.-Y. and M. Bouchon (1980a). The seismic response of sediment-filled valleys, Part 1. The case of incident SH-waves, *Bulletin Seismological Society of America*, 70, 1263-1286.
- Bard, P.-Y. and M. Bouchon (1980b). The seismic response of sediment-filled valleys, Part 2. The case of incident P- and SV-waves, *Bulletin Seismological Society of America*, 70, 1921-1941.
- Barka, A. and K. Kadinsky-Cade (1988). Strike-slip fault geometry in Turkey and its influence on earthquake activity, *Tectonics*, 7, 663-684.
- Barka, A. and I. Kuscü (1996). Extends of the North Anatolian Fault in the Izmit, Gemlik and Bandirma Bays, *Turkish Journal Marine Science*, 2, 93-106.
- Barka, A. (1997). Neotectonics of the Marmara region, active tectonics of Northwestern Anatolia-the Marmara poly-project, a multidisciplinary approach by space-geodesy, geology, hydrogeology, geothermics and seismology, vdf Hochschulverlag AG an der ETH Zurich, 55-87.
- Chavez-Garcia, F.J. and E. Faccioli (2000). Complex site effects and building codes: making the leap, *Journal of Seismology*, 4(1), 23-40.
- Choi, Y., J.P. Stewart and R.W. Graves (2005). Empirical model for basin effects accounts for basin depth and source location, *Bulletin Seismological Society of America*, 95, 412-427.
- Dewey, J.F. and A.M.C. Sengor (1979). Aegean and surrounding regions: complex multi-plate and continuum tectonics in a convergent zone, *Geological Society of America Bulletin*, 90, 84-92.
- Field, E.H. (1996). Spectral amplification in a sediment-filled valley exhibiting clear basin-edge-induced waves, *Bulletin Seismological Society of America*, 86, 991-1005.
- Flerit, F., R. Armijo, G. King, B. Meyer and A. Barka (2003). Slip partitioning in the Sea of Marmara pull-apart determined from GPS velocity vectors, *Geophysical Journal International*, 154, 1-7.
- Graves, R.W., A. Pitarka and P.G. Somerville (1998). Ground-motion amplification in the Santa Monica area: effects of shallow basin-edge structure, *Bulletin Seismological Society of America*, 88, 1224-1242.
- Hruby, C.E. and I.A. Beresnev (2003). Empirical corrections for basin effects in stochastic ground-motion prediction, based on the Los Angeles basin analysis, *Bulletin Seismological Society of America*, 93, 1679-1690.
- Imbach, T. (1997) Geology of Mount Uludag with emphasis on the genesis of the Bursa, Northwest Anatolia, Turkey, In: *Active Tectonics of Northwestern Anatolia-The Marmara Poly-Project*, (eds. Shindler, C. and Pfister, M.) (Hochschulverlag AG an der ETH Zurich-Swiss), 239-266.
- Irmak, T.S., H. Grosser, M.F. Ozer, H. Woith and S. Baris (2007). The 24 October 2006 Gemlik Earthquake (M=5.2), *Geophysical Research Abstracts*, 9, 10212.
- Karabulut, H., J. Schmittbuhl, S. Ozalaybey, O. Lengliné, A. Komec-Mutlu, V. Durand, M. Bouchon, G. Daniel and M.P. Bouin (2011). Evolution of the seismicity in the eastern Marmara Sea a decade before and after the 17 August 1999 Izmit earthquake, *Tectonophysics*, 510, 17-27.
- Kawase, H. (1996). The cause of the damage belt in Kobe: "the basin-edge effect" constructive interference of the direct S-wave with the basin-induced diffracted/rayleigh waves, *Seismological Research Letters*, 67, 25-34.
- Kinscher, J., F. Krüger, H. Woith, B.G. Luhr, E. Hintersberger, T.S. Irmak and S. Baris (2013). Seismotectonics of the Armutlu peninsula (Marmara Sea, NW Turkey) from geological field observation and regional moment tensor inversion, *Tectonophysics*, 608, 980-995.
- Konno, K. and T. Ohmachi (1998). Ground-motion characteristics estimated from spectral ratio between horizontal and vertical components of microtremor, *Bulletin Seismological Society of America*, 88, 228-241.
- Kurtulus, C. and M.M. Canbay (2007). Tracing the middle strand of the North Anatolian Fault Zone through the southern Sea of Marmara based on seismic reflection studies, *Geo-Marine Letters* 27, 27-40.
- Kuscü, I., M. Okamura, H. Matsuoka, K. Yamamori, Y. Awata and S. Ozalp (2009). Recognition of active faults and stepover geometry in Gemlik Bay, Sea of Marmara, NW Turkey, *Marine Geology*, 260, 90-101.

- Le Pichon, X., A.M.C. Sengor, E. Demirbag, C. Rangin, C. Imren, R. Armijo, N. Gorur, N. Cagatay, B. Mercier de Lepinay, B. Meyer, R. Saatçilar and B. Tok, (2001). The active Main Marmara Fault, *Earth Planet Sci Lett*, 192 (4), 543-560.
- Makra, K., D. Raptakis, F.J. Chavez-Garcia and K. Pitilakis (2001). Site effects and design provisions: The case of Euroseistest, *Pure and Applied Geophysics*, 158, 2349-2367.
- Makra, K., F.J. Chavez-Garcia, D. Raptakis, and K. Pitilakis (2005). Parametric analysis of the seismic response of a 2D sedimentary valley: implications for code implementations of complex site effects, *Soil Dynamics and Earthquake Engineering* 25, 303-315.
- McClusky, S., S. Balassanian, A. Barka, C. Demir, S. Ergintav, I. Georgiev, O. Gurkan, M. Hamburger, K. Hurst, H. Kahle, K. Kastens, K. Kekelidze and R. King (2000). Global positioning system constraints on plate kinematics and dynamics in the eastern Mediterranean and Caucasus, *Journal of Geophysical Research*, 105, 5695-5719.
- Meade, B.J., B.H. Hager, R.E. McClusky, S. Reilinger, S. Ergintav, O. Lenk, A. Barka and H. Ozener (2002). Estimates of seismic potential in the Marmara region from block models of secular deformation constrained by global positioning system measurements, *Bulletin Seismological Society of America*, 92, 208-215.
- Miksat, J., F. Wenzel and V. Sokolov (2005). Low free-field accelerations of the 1999 Kocaeli earthquake, *Pure and Applied Geophysics*, 162, 857-874.
- Nakamura, Y. (1989). A method for dynamic characteristics estimation of subsurface using microtremor on the ground surface, *QR Rail Tech Res Inst*, 30, 25-30.
- Narayan, J.P. (2005). Study of basin-edge effects on the ground motion characteristics using 2.5-D modeling, *Pure and Applied Geophysics*, 162, 273-289.
- Nyst, M. and W. Thatcher (2004). New constraints on the active tectonic deformation of the Aegean, *Journal of Geophysical Research*, 109, B11406:23. doi:10.1029/2003JB002830.
- Olsen, K.B., R. Nigbor and T. Konno (2000). 3D viscoelastic wave propagation in the upper Borrego valley, California, constrained by borehole and surface data, *Bulletin Seismological Society of America*, 90, 134-150.
- Orgulu, G. (2011). Seismicity and source parameters for small-scale earthquakes along the splays of the North Anatolian Fault (NAF) in the Marmara Sea, *Geophysical Journal International*, 184, 385-404.
- Ozbey, C., A. Sari, L. Manuel, M. Erdik and Y. Fahjan (2004). An empirical attenuation relationship for northerwestern Turkey ground motion using a random effects approach, *Soil Dynamics and Earthquake Engineering*, 24, 115-125.
- Reipl, J., J. Zahradnik, V. Plicka and P.-Y. Bard (2000). About the efficiency of numerical 1-D and 2-D modeling of site effects in basin structures, *Pure and Applied Geophysics*, 157, 319-342.
- Sandikkaya, M.A., M.T. Yilmaz, B.B. Bakir and O. Yilmaz (2010). Site classification of Turkish national strong-motion stations, *Journal of Seismology*, 14, 543-563.
- Saroglu, F., O. Emre and I. Kuscü (1992). Active Fault Map of Turkey, 1:1000 000 scale, 3 sheets, MTA publ, Ankara.
- Sengor, A.M.C., N. Gorur and F. Saroglu (1985). Strike-slip faulting and related basin formation in zones of tectonic escape: Turkey as a case study, In: Biddle KT, Christie-Blick N (Eds), *Strike-slip Deformation, Basin Formation, and Sedimentation*. Society of Economical Paleontology and Mineralogy Special Publication, 37, 227-264.
- Shakal, A., H. Haddadi, V. Graizer, K. Lin and M. Huang (2006). Some key features of the strong-motion data from the M 6.0 Parkfield, California, earthquake of 28 September 2004, *Bulletin Seismological Society of America*, 96, S90-S118.
- Smith, A.D., T. Taymaz, F.Y. Oktay, H. Yuçe, B. Alpar, H. Basaran, J.A. Jackson, S. Kara and M. Simsek (1995). High-resolution seismic profiling in the Sea of Marmara (Northwest Turkey): Late Quaternary sedimentation and sea-level changes, *Geological Society of America Bulletin*, 107, 923-936.
- Tunc, B., D. Caka, T.S. Irmak, H. Woith, S. Tunc, S. Baris, M.F. Ozer, B.G. Luhr, E. Gunther, H. Grosser and J. Zschau (2011). The Armutlu Network: an investigation into the seismotectonic setting of Armutlu-Yalova-Gemlik and the surrounding regions, *Annals of Geophysics*, 54 (1), 35-45.
- Wang, G.-Q., G.-Q. Tang, C.R. Jackson, X.-Y. Zhou and Q.-L. Lin (2006). Strong ground motions observed at the UPSAR during the 2003 M6.5 San Simeon and 2004 M6.0 Parkfield, California, Earthquakes, *Bulletin Seismological Society of America*, 96, S159-S182.
- Wen, K.-L., H.-Y. Peng, Y.-B. Tsai and K.C. Chen (2001). Why 1G was recorded at TCU129 site during the 1999 Chi-Chi, Taiwan earthquake, *Bulletin Seismological Society of America*, 91, 1255-1266.
- Yalcinkaya, E. and O. Alptekin (2005a). Contributions of the basin edge induced surface waves to site effect in the Dinar Basin, Southwestern Turkey, *Pure and Applied Geophysics*, 162, 931-951.
- Yalcinkaya, E. and O. Alptekin (2005b). Numerical 2D modeling of site response in Dinar Graben, South-

west Turkey, and comparison with observations,
Annals of Geophysics, 48 (2), 247-258.

Yalcinkaya, E., A. Pinar, O. Uskuloglu, S. Tekebas and B. Firat (2012). Selecting the most suitable rupture model for the stochastic simulation of the 1999 Izmit earthquake and prediction of peak ground motions, *Soil Dynamics and Earthquake Engineering*, 42, 1-16.

*Corresponding author: Esref Yalcinkaya,
Istanbul University, Engineering Faculty, Geophysical Engineering, Avcilar, Istanbul, Turkey; email: eyalcin@istanbul.edu.tr.